J. Phys. B: At. Mol. Opt. Phys. **42** (2009) 175501 (10pp) doi:10.1088/0953-4075/42/17/175501

Frequency locking of an optical cavity using linear–quadratic Gaussian integral control

S Z Sayed Hassen[1], M Heurs[1], E H Huntington[1], I R Petersen[1] and M R James[2]

[1] School of Information Technology and Electrical Engineering, University of New South Wales at the Australian Defence Force Academy, Canberra, ACT 2600, Australia
[2] Department of Engineering, Australian National University, Canberra, ACT 2600, Australia

E-mail: s.sayedhassen@student.adfa.edu.au

Received 1 October 2008, in final form 14 July 2009
Published 10 August 2009
Online at stacks.iop.org/JPhysB/42/175501

Abstract
We show that a systematic modern control technique such as linear–quadratic Gaussian (LQG) control can be applied to a problem in experimental quantum optics which has previously been addressed using traditional approaches to controller design. An LQG controller which includes integral action is synthesized to stabilize the frequency of the cavity to the laser frequency and to reject low frequency noise. The controller is successfully implemented in the laboratory using a dSpace digital signal processing board. One important advantage of the LQG technique is that it can be extended in a straightforward way to control systems with multiple measurements and multiple feedback loops. This work is expected to pave the way for extremely stable lasers with fluctuations approaching the quantum noise limit and which could be potentially used in a wide range of applications.

(Some figures in this article are in colour only in the electronic version)

1. Introduction

Fundamental interest, as well as a variety of potential applications, is driving research beyond the observation of the physics of quantum systems and towards their precise control and manipulation. It is somewhat of a truism to observe that feedback can change the dynamics of a physical system. Indeed many experiments involving quantum systems rely on feedback control for their success. The frequency-and-intensity-stabilized laser that is commonly used as a source in quantum optics experiments is an excellent example of this notion. Examples of other quantum systems in which feedback control will play a key role include the quantum error correction problem [1], control of atom lasers and Bose–Einstein condensates [2], and the feedback cooling of a nanomechanical resonator [3]. Here we shall focus our attention on quantum-optical systems.

When the role of feedback is explicitly considered in quantum-optical experiments, it is usually done so in the context of determining the ultimate limit of performance under closed-loop operation. For example, Yamamoto *et al* [4] showed that the freely propagating output of any feedback loop based on a beamsplitter must have noise greater than the quantum noise limit. Considerable attention has also been paid to the physics of various measurement signals that might be used as the input to the feedback controller. Seminal examples of this research include the discoveries of the Pound–Drever–Hall and Hänsch–Coulliaud error signals [5, 6].

Such issues are unquestionably important, but a number of interesting open questions remain. For example, how does one define the optimal performance of the controlled system when there are multiple, often competing design objectives? Based on the measurement technique used, the design objectives and the physics of the system under control (the plant), what is the optimal (in a global sense) controller to use? How are the physical constraints of the plant, measurement and controller incorporated into that optimal design? How are uncertainties in our understanding of the plant included in the controller design and how do they affect the physics of the controlled system?

 © 2009 IOP Publishing Ltd Printed in the UK

In-principle answers to many of these questions may be found from systematic control techniques such as optimal parameter estimation, Kalman filtering, robust controller design, $\mathcal{H}^\infty$ controller design and linear–quadratic-Gaussian (LQG) controller design [7–10]. One point of commonality for all of these techniques is that a design objective is defined mathematically, from which optimal dynamics may be determined and then implemented. A highly analogous set of optimal control techniques has been applied to open-loop control of a variety of quantum systems (see [11] and references therein), with a profound impact on their ability to demonstrate fundamental quantum information processing concepts.

In this paper, we demonstrate the use of systematic methods of LQG optimal control to frequency-lock an optical cavity. Investigation of this deceptively simple quantum-optical system under feedback control provides insight into a number of the open questions listed above. For example, the LQG cost functional codifies the optimal performance of the controlled system, under experimentally realistic constraints. As discussed later, this experiment is unusual in that the desired physics of the closed-loop cavity lead to the specific choice of an integral LQG cost functional [12], rather than the regular LQG cost functional [13]. Additionally, the use of optimal estimation techniques leads to the design of the optimal controller under those constraints.

More specifically, a linear dynamical model of the empty cavity is obtained using both physical considerations and experimentally measured frequency response data. The data are fitted to the model using a subspace system identification method [14]. Homodyne detection of the reflected port of a Fabry–Perot cavity is used as the measurement signal for the controller. The integral LQG controller design is discretized and implemented on a dSpace digital signal processing (DSP) system, and experimental results were obtained. We show that the controller was effective in locking the optical cavity to the laser frequency, and that the physical response of the cavity under feedback control (as quantified by the step response) is as predicted.

This paper is structured as follows: in section 2, the quantum-optical model of an empty cavity is formulated in a manner consistent with the LQG design methodology; section 3 outlines the experimental setup upon which the LQG design methodology is used; section 4 outlines the subspace system identification technique used to arrive at the linear dynamic model for the cavity system; section 5 presents the LQG optimal controller design methodology as applied to the problem of locking the frequencies of a laser and empty cavity together; section 6 presents experimental results; and we conclude in section 7.

2. Cavity model

A schematic of the frequency stabilization system is depicted in figure 1.

The cavity can be described in the Heisenberg picture by the following quantum stochastic differential equations; e.g., see [15] and section 9.2.4 of [16]:

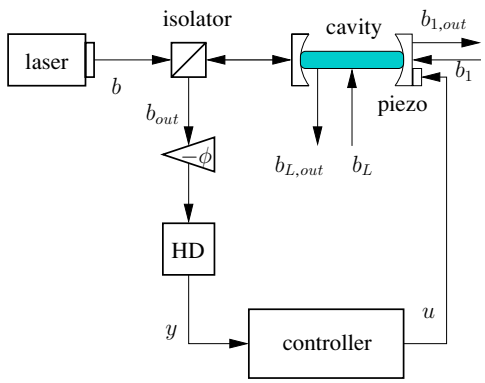

Figure 1. Cavity locking feedback control loop. The phase quadrature of the reflected field b_{out} is measured using homodyne detection. The measured signal is fed into a digital controller which generates a control signal u and actuates a piezo-electric transducer. This controls the position of one of the cavity mirrors and adjusts the length of the cavity.

$$\dot{a} = -\left(\frac{\kappa}{2} + \mathrm{i}\Delta\right)a - \sqrt{\kappa}_0(\beta + b_0) - \sqrt{\kappa}_1 b_1 - \sqrt{\kappa}_{\mathrm{L}} b_{\mathrm{L}},$$
$$b_{\text{out}} = \sqrt{\kappa}_0 a + \beta + b_0. \tag{1}$$

Here, the annihilation operator for the cavity mode is denoted by a and the annihilation operator for the coherent input mode is denoted by $b = \beta + b_0$, both defined in an appropriate rotating reference frame, where b_0 is quantum noise. We have written $\kappa = \kappa_0 + \kappa_1 + \kappa_{\mathrm{L}}$, where κ_0, κ_1 and κ_{L} quantify the strength of the couplings of the respective optical fields to the cavity, including the losses. The input to the cavity is taken to be a coherent state with amplitude β and which is assumed to be real. The assumption of a coherent state is well justified because homodyne detection cancels out any common-mode quadrature amplitude and phase variations in the laser. Δ denotes the frequency detuning between the laser frequency and the resonant frequency of the cavity. The objective of the frequency stabilization scheme is to maintain $\Delta = 0$. The detuning is given by

$$\Delta = \omega_{\mathrm{c}} - \omega_{\mathrm{L}} = q\frac{2\pi c}{nL} - \omega_{\mathrm{L}}, \tag{2}$$

where ω_{c} is the resonant frequency of the cavity, ω_{L} is the laser frequency, nL is the optical path length of the cavity, c is the speed of light in a vacuum and q is a large integer indicating that the qth longitudinal cavity mode is being excited.

The cavity locking problem is formally a nonlinear control problem since the equations governing the cavity dynamics in (1) contain the nonlinear product term Δa. In order to apply linear optimal control techniques, we linearize these equations about the zero-detuning point. Let α denote the steady-state average of a when $\Delta = 0$ such that $a = \alpha + \tilde{a}$. The perturbation operator $\tilde{a}$ satisfies the linear quantum stochastic differential equation (neglecting higher order terms)

$$\dot{\tilde{a}} = -\frac{\kappa}{2}\tilde{a} - \mathrm{i}\Delta\alpha - \sqrt{\kappa}_0 b_0 - \sqrt{\kappa}_1 b_1 - \sqrt{\kappa}_{\mathrm{L}} b_{\mathrm{L}}. \tag{3}$$

The perturbed output field operator $\tilde{b}_{\text{out}}$ is given by

$$\tilde{b}_{\text{out}} = \sqrt{\kappa}_0\tilde{a} + b_0, \tag{4}$$

which implies $b_{\text{out}} = \sqrt{\kappa}_0\alpha + \beta + \tilde{b}_{\text{out}}$.

We model the measurement of the X_ϕ quadrature of $\tilde{b}_{\text{out}}$ with homodyne detection by changing the coupling operator for the laser mode to $\sqrt{\kappa}_0 e^{-i\phi}a$, and measuring the real quadrature of the resulting field. The measurement signal is then given by

$$\tilde{y} = \tilde{b}_{\text{out}} + \tilde{b}^\dagger_{\text{out}} = \sqrt{\kappa}_0(e^{-i\phi}\tilde{a} + e^{i\phi}\tilde{a}^\dagger) + q_0, \tag{5}$$

where $q_0 = b_0 + b_0^\dagger$ is the intensity noise of the input coherent state.

As we shall see in section 5, the LQG controller design process starts from a state-space model of the plant, actuator and measurement, traditionally expressed in the form:

$$\begin{aligned} \dot{x} &= Ax + Bu + D_1 w, \\ y &= Cx + D_2 w \end{aligned} \tag{6}$$

where x represents the vector of system variables (we shall not use the control engineering term 'states' to avoid confusion with quantum-mechanical states), u is the input to the system, y is the measured output and w is a Gaussian white noise disturbance acting on the system. Also, A represents the system matrix, B is the input matrix, C is the output matrix, and D_1 and D_2 are the system noise matrices.

The cavity dynamics and homodyne measurement are expressed in state-space form in terms of the quadratures of the operators $\tilde{a}, b_0, b_1, b_L$ as

$$\begin{aligned} \begin{bmatrix} \dot{\tilde{q}} \\ \dot{\tilde{p}} \end{bmatrix} &= \begin{bmatrix} -\frac{\kappa}{2} & 0 \\ 0 & -\frac{\kappa}{2} \end{bmatrix} \begin{bmatrix} \tilde{q} \\ \tilde{p} \end{bmatrix} + \begin{bmatrix} 0 \\ -2\alpha \end{bmatrix} \Delta \\ &\quad - \sqrt{\kappa}_0 \begin{bmatrix} \cos\phi & \sin\phi \\ -\sin\phi & \cos\phi \end{bmatrix} \begin{bmatrix} q_0 \\ p_0 \end{bmatrix} \\ &\quad - \sqrt{\kappa}_1 \begin{bmatrix} 1 & 0 \\ 0 & 1 \end{bmatrix} \begin{bmatrix} q_1 \\ p_1 \end{bmatrix} - \sqrt{\kappa}_L \begin{bmatrix} 1 & 0 \\ 0 & 1 \end{bmatrix} \begin{bmatrix} q_L \\ p_L \end{bmatrix}, \\ y &= k_2\sqrt{\kappa}_0 \begin{bmatrix} \cos\phi & \sin\phi \end{bmatrix} \begin{bmatrix} \tilde{q} \\ \tilde{p} \end{bmatrix} \\ &\quad + k_2 \begin{bmatrix} 1 & 0 \end{bmatrix} \begin{bmatrix} q_0 \\ p_0 \end{bmatrix} + w_2 = z + k_2 \begin{bmatrix} 1 & 0 \end{bmatrix} \begin{bmatrix} q_0 \\ p_0 \end{bmatrix} + w_2 \end{aligned} \tag{7}$$

with noise quadratures $q_j = b_j + b_j^\dagger$, $p_j = -i(q_j - p_j^\dagger)$, for $j = 0, 1, L$ (all standard Gaussian white noises). Here, y is the homodyne detector output in which we have included an electronic noise term w_2. Also, k_2 represents the transimpedance gain of the homodyne detector, including the photodetector quantum efficiency.

3. Experimental layout

Figure 2 illustrates the experimental setup in more detail. Approximately 1 mW of the 1064 nm, single-mode output of a diode-laser pumped, miniature monolithic Nd:YAG laser operating at 235 mW is used as the input to a linear cavity. Both mirrors of the linear cavity have 98% reflectivity, with the input coupler (the mirror closest to the laser) being plane, the output coupler having a 300 mm radius of curvature and the mirrors being separated by a nominal 200 mm. Such a cavity has a free-spectral range of 750 MHz, a finesse of approximately 150 and a waist of approximately 220 μm, located at the input coupler to the cavity [17, 18].

The field reflected from the cavity is extracted via an optical circulator. The circulator is implemented with a mirror with 2 mm aperture in its centre, a calcite beam displacer and a quarter-wave plate placed immediately prior to the input coupler of the cavity. That arrangement is used rather than the more usual polarizing beamsplitter and quarter-wave plate combination as it provides a co-propagating, and hence automatically phase-locked, local oscillator for the homodyne detection system. As indicated in figure 2, the local oscillator does not excite any modes of the optical cavity, it simply reflects off the input coupler to the cavity.

The fringe visibility of the homodyne detection system is measured to be greater than 98%. Less than 5% of power is measured in higher order modes of the cavity. The length of the cavity, and hence its resonant frequency, is actuated via a tubular piezo-electric transducer, PZT (with a stroke of 10 μm when the maximum 500 V was applied) to which the output coupler is mounted.

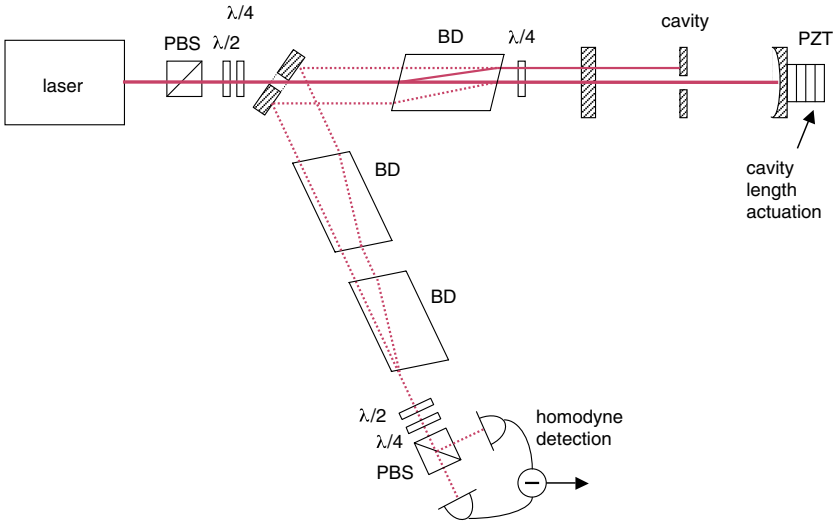

Figure 2. Detailed schematic of the experimental setup. Acronyms and symbols are BD = beam displacer; $\lambda/4$ = quarter-wave plate; $\lambda/2$ = half-wave plate; PBS = polarizing beamsplitter; PZT = piezo-electric transducer. Dashed lines denote the field reflected from the cavity.

In the nomenclature of the sections to follow, the system illustrated in figure 2 is the 'plant' with the homodyne detector output being the measurement signal y and the input voltage applied to the high-voltage amplifier driving the PZT being the control signal u. Experimental results presented in the remainder of this paper all pertain to the system outlined in this section.

4. System identification

The state-space model of the cavity given in (7) is incomplete as it does not include an explicit model, including the actuation mechanism, for the dynamics of the detuning, Δ. The dynamics of the detuning and actuation mechanism are sufficiently complex that direct measurement is a more experimentally reasonable approach than *a priori* modelling of the system. The process of obtaining a mathematical model of the system to be controlled directly from measured data for that system is known as system identification.

It is at this point that the controller design process diverges from traditional, pre-1960s control techniques. Specifically, in the traditional approach, a controller is designed using root-locus or frequency response methods, based on measurements of the plant transfer function [19]. In the modern control approach, a system identification method is used to determine a state-space model from the input–output frequency response data and generates the system matrices A, B and C in (6); see [20]. The system matrices are used in the LQG design process as we shall see in section 5. The method of system identification which is applied in this paper is the frequency domain subspace system identification method. We now provide a brief overview of the subspace system identification method.

4.1. Subspace system identification

The frequency domain subspace system identification method enables the matrices A, B and C in the state-space model (6) to be constructed from measurements of the system frequency response. The transfer function of the system (6) is given by $G(s) = C(sI - A)^{-1}B$, where I is the identity matrix. The measured frequency response data are assumed to take the form of a set of noisy measurements of this transfer function evaluated at a range of discrete frequency points:

$$G_k = G(j\omega_k) + n_k, \qquad k = 1, 2, \ldots, N. \tag{8}$$

In practice, the measured frequency response data can be obtained using an instrument such as a swept sine digital signal analyser. The frequency domain subspace system identification method is a non-iterative method of constructing the state-space matrices A, B and C from the frequency response data $G_k, k = 1, 2, \ldots, N$.

The subspace system identification method is based on the realization theory of [21, 22] which involved constructing a state-space model using impulse response data. This approach was generalized to allow for general time domain input–output data in the papers [23, 24] and the resulting system identification method is referred to as the time domain subspace method. A frequency domain counterpart to this approach was first proposed in [25] and the actual algorithm implemented in this paper is based on the more recent paper [14].

We now outline the main steps in the frequency domain subspace system identification method of [14] which was applied in this paper. The first step is to convert the frequency domain data (8) into frequency domain data for a corresponding discrete time system via a bilinear tranformation:

$$\check{G}_k = G_k, \qquad k = 1, 2, \ldots, N,$$
$$\check{\omega}_k = 2\tan^{-1}\left(\frac{\omega_k T}{2}\right) k = 1, 2, \ldots, N. \tag{9}$$

This operation, which simply involves scaling the frequency values, is carried out because direct application of the subspace method to the continuous-time frequency response data would lead to severe numerical problems; see [26]. The scaling 'time constant' T is typically chosen to be the reciprocal of the maximum frequency of the available frequency response data: $T = \frac{2\pi}{\omega_N}$.

The next step is to use the discrete time–frequency response data to construct the matrices

$$G = \frac{1}{\sqrt{N}}\begin{bmatrix} \check{G}_1 & \check{G}_2 & \ldots & \check{G}_N \\ \mathrm{e}^{\mathrm{j}\check{\omega}_1}\check{G}_1 & \mathrm{e}^{\mathrm{j}\check{\omega}_2}\check{G}_2 & \ldots & \mathrm{e}^{\mathrm{j}\check{\omega}_N}\check{G}_N \\ \mathrm{e}^{\mathrm{j}2\check{\omega}_1}\check{G}_1 & \mathrm{e}^{\mathrm{j}2\check{\omega}_2}\check{G}_2 & \ldots & \mathrm{e}^{\mathrm{j}2\check{\omega}_N}\check{G}_N \\ \vdots & \vdots & \ddots & \vdots \\ \mathrm{e}^{\mathrm{j}(q-1)\check{\omega}_1}\check{G}_1 & \mathrm{e}^{\mathrm{j}(q-1)\check{\omega}_2}\check{G}_2 & \ldots & \mathrm{e}^{\mathrm{j}(q-1)\check{\omega}_N}\check{G}_N \end{bmatrix},$$

$$W = \frac{1}{\sqrt{N}}\begin{bmatrix} I & I & \ldots & I \\ \mathrm{e}^{\mathrm{j}\check{\omega}_1}I & \mathrm{e}^{\mathrm{j}\check{\omega}_2}I & \ldots & \mathrm{e}^{\mathrm{j}\check{\omega}_N}I \\ \mathrm{e}^{\mathrm{j}2\check{\omega}_1}I & \mathrm{e}^{\mathrm{j}2\check{\omega}_2}I & \ldots & \mathrm{e}^{\mathrm{j}2\check{\omega}_N}I \\ \vdots & \vdots & \ddots & \vdots \\ \mathrm{e}^{\mathrm{j}(q-1)\check{\omega}_1}I & \mathrm{e}^{\mathrm{j}(q-1)\check{\omega}_2}I & \ldots & \mathrm{e}^{\mathrm{j}(q-1)\check{\omega}_N}I \end{bmatrix}.$$

From these matrices, the matrices $\check{A}$ and $\check{C}$ from the discrete time state-space model are constructed via the use of various linear algebra operations including QR factorization and singular value decomposition; see e.g. [27]. Then the matrices $\check{B}$ and $\check{D}$ from the discrete time state–space model are constructed by solving the least squares problem:

$$\min_{\check{B},\check{D}} \sum_{k=1}^{N} \left\| \check{G}_k - \check{D} - \check{C}(\mathrm{e}^{\mathrm{j}\omega_k} I - \check{A})^{-1}\check{B} \right\|_{\mathrm{F}}^2,$$

where the notation $\|\cdot\|_{\mathrm{F}}$ denotes the matrix Frobenious norm. Then the required continuous time state-space matrices are constructed according to the bilinear transformation formulae:

$$A = \frac{2}{T}\left(I + \check{A}\right)^{-1}\left(\check{A} - I\right), \qquad B = \frac{2}{\sqrt{T}}\left(I + \check{A}\right)^{-1}\check{B},$$
$$C = \frac{2}{\sqrt{T}}\check{C}\left(I + \check{A}\right)^{-1}, \qquad D = \check{D} - \check{C}\left(I + \check{A}\right)^{-1}\check{B}.$$

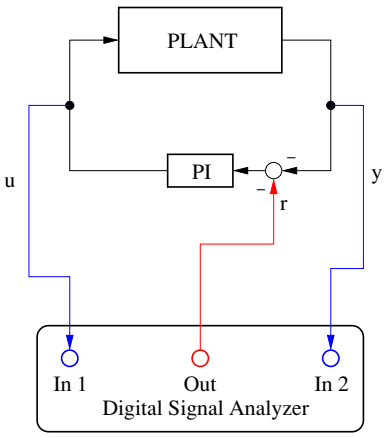

Figure 3. Experimental set up used to measure the plant frequency response. In this experimental set up, an analogue PI controller is used to stabilize the system and a digital signal analyser is used to obtain the plant frequency response data.

4.2. Subspace identification of the cavity system

The transfer function of the cavity and measurement system described in section 3 (or alternatively the 'plant') is identified under closed-loop conditions. We use an analogue proportional-integral (PI) controller to stabilize the system for the duration of the measurement. The experimental setup in which a digital signal analyser was used to measure the plant frequency response data is shown in figure 3. In particular, the digital signal analyser which is used to measure the plant frequency response excites the system with a series of sinusoidal inputs at a discrete set of frequencies and correlates the sinusoidal input signal with the sinusoidal plant output signal in order to determine the gain and phase of the system frequency response at each frequency. The frequency response data thus obtained for the plant are plotted in figure 4. From the data, at least three resonances can be clearly identified, occurring at frequencies of about 520, 2100 and 5000 Hz, respectively.

An eighth-order anti-aliasing filter with a corner frequency of 2.5 kHz (chosen because it is far greater than the unity-gain bandwidth of the controller and far less than the 50 kHz sampling frequency) was placed immediately prior to the digital LQG controller. Such filters are commonly used in digital control systems (e.g., see [28]) in order to ensure that the bandwidth of the signal being sampled satisfies the Nyquist condition. The anti-aliasing filter is regarded as augmenting the plant so that the augmented plant has a frequency response that is the product of the plant data gathered previously and the anti-aliasing filter which is identified separately.

The frequency response data obtained are then used to determine a 13th-order model (that is the vector x in (6) is of dimension 13) using the frequency domain subspace identification method of [14]. Figure 5 compares the gain (in decibels) and the phase (in degrees) of the measured frequency data for the augmented plant with that of the identified system model.

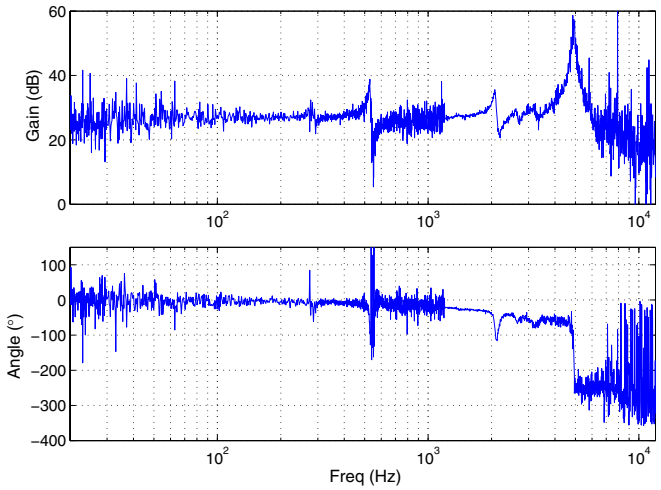

Figure 4. Measured plant frequency response. This frequency response corresponds to the transfer function of the cavity system from the input signal u applied to the PZT to the output signal y measured using Homodyne detection.

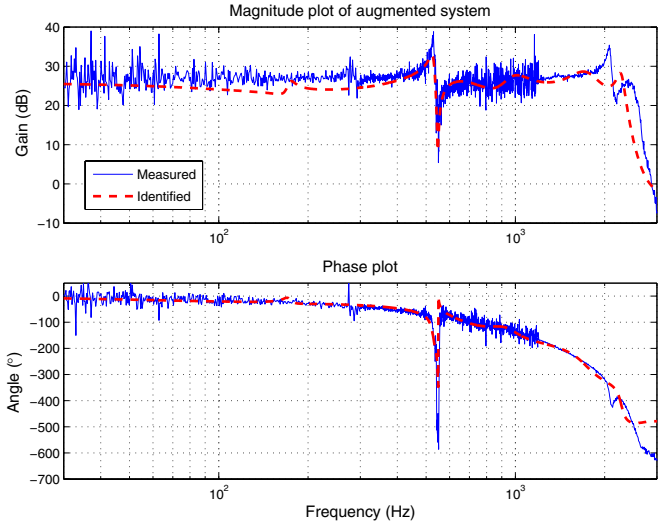

Figure 5. Measured frequency response data for the augmented plant and frequency response for the identified system model. The augmented plant consists of the cavity system, whose frequency response is illustrated in figure 4, cascaded with a low-pass anti-aliasing filter, which suppresses the plant resonances above 2.5 kHz. The identified system model was constructed from the augmented plant measured frequency response data using the subspace system identification method.

5. Linear quadratic Gaussian optimal control

The solution to the LQG optimal control problem originated with the work of Kalman. In the paper [29], the state feedback linear–quadratic optimal control problem was solved in terms of Riccati equations. Also, in the papers [30, 31], the optimal state estimation problem was solved using a method which has become known as the Kalman–Bucy filter. A combination of the methods of [29, 31] leads to the solution of the LQG optimal control problem.

The LQG optimal control approach to controller design begins with a linear state-space model of the form (6). Note

that this model involves the use of Gaussian white noise disturbances although a more rigorous formulation of the LQG optimal control problem involves the use of a Wiener process to describe the noise rather than the white noise model (6); e.g., see [32]. However, for the purposes of this paper, a model of the form (6) is most convenient. In the model (6), the term $D_1 w$ corresponds to the process noise and the term $D_2 w$ corresponds to the measurement noise. The LQG optimal control problem involves constructing a dynamic measurement feedback controller to minimize a quadratic cost functional of the form

$$\mathcal{J} = \lim_{T\to\infty} \mathbf{E}\left[\frac{1}{T}\int_0^T [x^T Q x + u^T R u]\mathrm{d}t\right], \qquad (10)$$

where $Q \geqslant 0$ and $R > 0$ are symmetric weighting matrices. The term $x^T Q x$ in the cost functional (10) corresponds to a requirement to minimize the system variables of interest and the term $u^T R u$ corresponds to a requirement to minimize the size of the control inputs. The matrices Q and R are chosen so that the cost functional reflects the desired performance objectives of the control system. The great advantage of the LQG optimal control approach to controller design is that it provides a tractable systematic way to construct output feedback controllers (even in the case of multi-input multi-output control systems). Also, numerical solutions exist in terms of algebraic Riccati equations which can be solved using standard software packages such as Matlab; e.g., see [13, 33]. A feature of the solution to the LQG optimal control problem is that it involves a Kalman filter which provides an optimal estimate $\hat{x}$ of the vector of system variables x based on the measured output y. This is combined with a 'state-feedback' optimal control law which is obtained by minimizing the cost functional (10) as if the vector of system variables x was available to the controller.

Note that the LQG controller design methodology does not directly address some important engineering issues in control system design such as controller bandwidth and the robustness of the control system against variations in the plant dynamics and errors in the plant model. These issues can however be taken into account in the controller design process by suitable choice of the noise terms in the plant model and by suitably choosing the quadratic cost functional (10). In this engineering approach to controller design, the LQG methodology is used to synthesize the controller on the basis of a model of the form (6) where the matrices A, B, C are determined from measurements made on the system but the matrices D_1 and D_2 are chosen so that the LQG controller has the required bandwidth and robustness characteristics. This approach has the advantage that it avoids the difficult problem of determining the matrices D_1 and D_2 from measurements or first principles modelling. Also, it ensures that the LQG controller which is designed will have a suitable bandwidth and level of robustness.

5.1. LQG performance criterion and integral action

The dynamics of the cavity and measurement system can be subdivided as shown in figure 6 and comprises an electro-mechanical subsystem and an electro-optical subsystem (the optical cavity and homodyne detector).

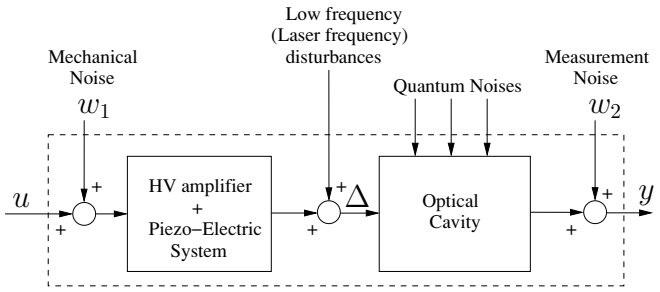

Figure 6. Block diagram of the plant showing all the noises and their respective point of entry into the plant. We will design an LQG feedback controller which takes measured values of the signal y and produces values of the control signal u such that the effect of the noises on Δ is minimized.

The control objective is to minimize the cavity detuning Δ, which is not available for measurement. Instead, the measurement signal y is the output of the homodyne detector and to include Δ in the performance criterion, we need to relate Δ to z. It can be seen from (7) that the transfer function of the optical cavity from Δ to z is a first-order low-pass filter with a corner frequency of $\kappa/2$. Physically, this arises from the well-known (see, for example [18, 34] and references therein) transfer function of the optical cavity from Δ to a phase shift, which is then measured by the homodyne detector. In the experimental system described herein $\kappa/2 \approx 10^6$ Hz, which is well beyond the frequency range of interest for the integral LQG controller. Hence we can consider z to be proportional to Δ under these conditions, and therefore minimizing variations in Δ can be regarded as being equivalent to minimizing variations in z.

The LQG performance criterion to be used for our problem is chosen to reflect the desired control system performance. That is, (i) to keep the cavity detuning Δ small (ideally zero) and (ii) to limit the control energy. However, these requirements are not sufficient to generate a suitable controller as the system is subject to a large initial dc offset and slowly varying disturbances. Our application requires the elimination of such effects. This can be achieved by using integral action and is the reason for our use of the integral LQG controller design method.

We include integral action by adding an additional term to the cost function given in (10) which involves the integral of the quantity z. Moreover, we include the 'integral state' as another variable of the system. The new variable $\int z\,\mathrm{d}t$ is also fed to the Kalman filter, which when combined with an optimal state-feedback control law leads to an integral LQG optimal controller. This controller will then meet the desired performance requirements as described above; e.g., see [12].

Figure 7 shows the integral LQG controller design configuration.

The overall system can be described in the state-space form as follows:

$$\dot{\tilde{x}} = \tilde{A}\tilde{x} + \tilde{B}u + \tilde{B}w_1, \qquad \tilde{y} = \tilde{C}\tilde{x} + \begin{bmatrix} w_2 \\ w_3 \end{bmatrix}, \qquad (11)$$

where

$$\tilde{x} = \begin{bmatrix} x \\ \int z\,\mathrm{d}\tau \end{bmatrix} \qquad \text{and} \qquad \tilde{y} = \begin{bmatrix} y_1 \\ y_2 \end{bmatrix}.$$

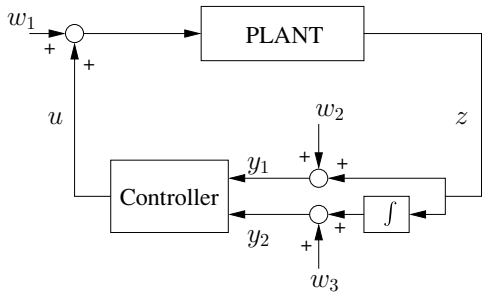

Figure 7. LQG integral controller design configuration. In this approach, integral action is ensured by providing a second measurement signal y_2 to the controller which is the integral of the output signal z. The integrator is then implemented as part of the overall LQG integral controller.

Here the matrices $\tilde{A}$, $\tilde{B}$, $\tilde{C}$ are constructed from the matrices A, B, C as follows:

$$\tilde{A} = \begin{bmatrix} A & 0 \\ C & 0 \end{bmatrix}, \qquad \tilde{B} = \begin{bmatrix} B \\ 0 \end{bmatrix} \qquad \text{and} \qquad \tilde{C} = \begin{bmatrix} C & 0 \\ 0 & I \end{bmatrix}.$$

Section 4 outlines the technique used to determine A, B, C.

In equation (11), the quantity w_1 represents mechanical noise entering the system which is assumed to be Gaussian white noise with variance ϵ_1^2. The quantity w_2 represents the sensor noise present in the system output y, which is assumed to be Gaussian white noise with variance ϵ_2^2. The quantity w_3 is included to represent the sensor noise added to the quantity $\int z\,\mathrm{d}t$. This is assumed to be Gaussian white noise with variance ϵ_3^2 and is included to fit into the standard framework for the LQG controller design. The parameters ϵ_1, ϵ_2 and ϵ_3 are treated as design parameters in the LQG controller design in section 5.2. There are a number of reasons for doing this. The first reason is that, as mentioned above, the LQG design methodology does not automatically guarantee that the resulting controller will have a suitable bandwidth or robustness properties. By suitably choosing the parameters ϵ_1, ϵ_2 and ϵ_3, these essential control engineering requirements can be satisfied. Also, the true variances of the noises w_1 and w_2 are not easy to determine in practice. In addition, the noise w_3 does not exist at all in the physical plant but has been added to the plant model in order to satisfy the mathematical requirements of the LQG controller synthesis procedure. Hence, there is no way to determine the 'true' variance of the noise w_3.

The general principles used in choosing ϵ_1, ϵ_2 and ϵ_3 are roughly as follows. The effect of increasing ϵ_1 or decreasing ϵ_2 and ϵ_3 is to increase the overall bandwidth of the control system. However, if the overall bandwidth of the control system is made too large, then this will result in a control system with poor robustness. Also, the relative size of ϵ_2 and ϵ_3 determines the amount of integral action in the control system. Decreasing ϵ_3 increases the amount of integral action.

The integral LQG performance criterion can be written as:

$$\mathcal{J} = \lim_{T\to\infty} \mathbf{E}\left[\frac{1}{T}\int_0^T [x^T Q x + L(z)^T \bar{Q} L(z) + u^T R u]\mathrm{d}t\right] \tag{12}$$

where

$$L(z) = \int_0^t z(\tau)\,\mathrm{d}\tau.$$

We choose the matrices Q, R and $\bar{Q}$ such that

$$x^T Q x = |z|^2, \qquad u^T R u = r|u|^2 \qquad \text{and} \qquad \bar{Q} = \bar{q},$$

where $r > 0$ and $\bar{q} > 0$ are also treated as design parameters.

The first term of the integrand in (12) ensures that the controlled variable z goes to zero, while the second term forces the integral of the controlled variable to go to zero. Also, the third term serves to limit the control input magnitude. The expectation in (12) is with respect to the classical Gaussian noise processes described previously and the assumed Gaussian initial conditions. Given our system as described by (11), the optimal LQG controller is given by (e.g., see [13])

$$u = -r^{-1}\tilde{B}^T X \hat{x} = F\hat{x}, \tag{13}$$

where X is the solution of the following matrix Riccati equation:

$$0 = X\tilde{A} + \tilde{A}^T X + \tilde{Q} - r^{-1} X\tilde{B}^T\tilde{B} X \tag{14}$$

and

$$\tilde{Q} = \tilde{C}^T \begin{bmatrix} 1 & 0 \\ 0 & \bar{q} \end{bmatrix} \tilde{C}.$$

Here $\hat{x}$ is an optimal estimate of the vector of plant variables $\tilde{x}$ obtained via a steady-state Kalman filter which can be described by the state equations

$$\dot{\hat{x}} = \tilde{A}\hat{x} + \tilde{B}u + K[\tilde{y} - \tilde{C}\hat{x}]. \tag{15}$$

For the case of uncorrelated process and measurement noises, the steady state Kalman filter is obtained by choosing the gain matrix K in (15) as

$$K = P\tilde{C}^T V_2^{-1}, \tag{16}$$

where P is the solution of the matrix Riccati equation

$$0 = \tilde{A}P + P\tilde{A}^T + V_1 - P\tilde{C}^T V_2^{-1}\tilde{C}P. \tag{17}$$

Here

$$V_1 = \epsilon_1^2\tilde{B}\tilde{B}^T = \mathbf{E}\big[w_1 w_1^T\big] \qquad \text{and} \qquad V_2 = \begin{bmatrix} \epsilon_2^2 & 0 \\ 0 & \epsilon_3^2 \end{bmatrix}$$

define the covariance of the process and measurement noises, respectively.

5.2. Design parameters

In designing the LQG controller, the parameters ϵ_1^2 (the mechanical noise variance), ϵ_2^2 (the sensor noise variance of y), ϵ_3^2 (the variance of the sensor noise added to $\int z$), r (the control energy weighting in the LQG cost function) and $\bar{q}$ (the integral output weighting in the LQG cost function) were used as design parameters and were adjusted for good controller performance. This includes a requirement that the control system has suitable gain and phase robustness margins and a reasonable controller bandwidth. The parameters were also chosen to ensure that the magnitude of the required control signal u was not too large. The specific values used for the design are shown in table 1:

Table 1. Design parameter values.

Design parameter	Value
ϵ_1	5×10^{-2}
ϵ_2	500
ϵ_3	3×10^{-4}
r	1×10^{3}
$\bar{q}$	1×10^{6}

5.3. Controller reduction

Using the design parameter values given in table 1, the LQG controller synthesis methodology leads to a 15th-order controller. That is, the vector $\hat{x}$ in the controller state equation (15) is of dimension 15. The digital implementation of such a high-order controller would require a long sampling time which would degrade the performance of the control system. Also, the use of such high-order controllers often leads to numerical problems when implemented digitally. Hence, it is desirable to approximate this 15th-order controller by a controller with a reduced state dimension.

In our case, we use a frequency-weighted balanced controller reduction approach to obtain a 6th-order controller. This approach allows for the inclusion of weighting transfer function matrices in the controller reduction process which put emphasis on a selected frequency range of interest. The new lower order model for the controller is determined by minimizing the weighted frequency response error between the original controller transfer function and the reduced controller transfer function; see [35]. Formally, the reduced-order controller is constructed so that the quantity

$$\left\| \frac{P(s)C(s)}{(I + P(s)C(s))}(C(s) - C_r(s)) \right\|_\infty \tag{18}$$

is minimized. Here, $P(s) = \tilde{C}(sI - \tilde{A})^{-1}\tilde{B}$, is the plant transfer function matrix and $C(s) = F(sI - \tilde{A} + K\tilde{C} - \tilde{B}F)^{-1}K$ is the original full controller transfer function matrix. Also, $C_r(s)$ is the reduced dimension controller transfer function matrix. The notation $\|M(s)\|_\infty$ refers to the $\mathcal{H}^\infty$ norm of a transfer function matrix $M(s)$ which is defined to be the maximum of $\sigma_{\max}[M(\mathrm{i}\omega)]$ over all frequencies $\omega \geqslant 0$. Here $\sigma_{\max}[M(\mathrm{i}\omega)]$ refers to the maximum singular value of the matrix $M(\mathrm{i}\omega)$. Figure 8 shows Bode plots of the full-order controller and the reduced-order controller.

Note that this approach to controller reduction does not guarantee the stability of the closed loop system with the reduced controller. We check for closed loop stability separately after the controller reduction process.

The reduced controller is then discretized at a sampling rate of 50 kHz and the corresponding Bode plot of the discrete-time loop gain is shown in figure 9. This discretized controller provides good gain and phase margins of 16.2 dB and 63°, respectively.

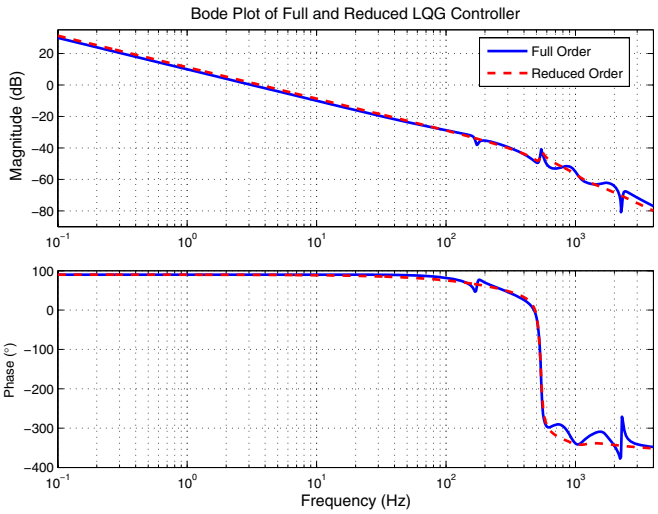

Figure 8. Bode plots showing the frequency response of the full-order (15th order) continuous LQG integral controller and the reduced-order (sixth order) continuous LQG integral controller. The reduced-order controller was constructed from the full-order controller using the frequency weighted balanced controller reduction method.

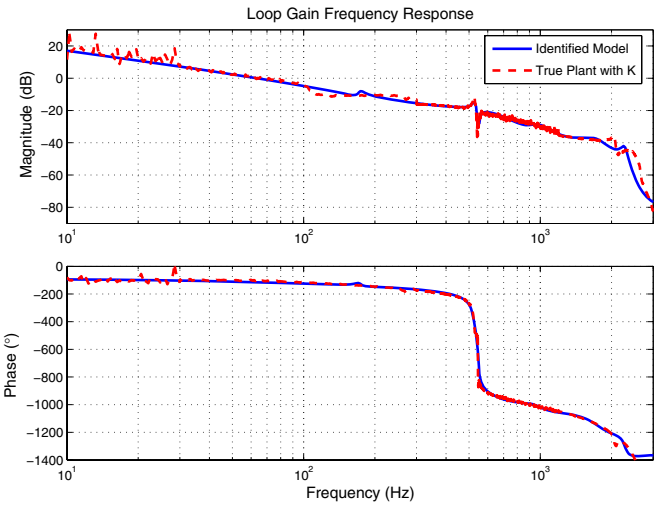

Figure 9. Bode plots of the loop gain transfer function $L(s)$. The loop gain transfer function is the product of the plant transfer function and the controller transfer function. The loop gain frequency response was constructed using both the measured plant frequency response data and the identified plant model transfer function. These Bode plots show that the controller provides a gain margin of 16 dB and 63° phase margin.

6. Experimental results and discussion

The discrete controller is implemented on a dSpace DS1103 Power PC DSP Board. This board is fully programmable from a Simulink block diagram and possesses 16-bit resolution. The controller successfully stabilizes the frequency in the optical cavity, locking its resonance to that of the laser frequency, f_0; see [36].

In addition, we also show that the control system is able to withstand significant disturbances which are introduced into the system. A step input of magnitude 0.1 V was applied to the closed-loop system. Figure 10 illustrates the experimental setup. Here, r is the step input signal and y is the resulting measured step response. The aim here is to show that the control system does not go out of lock as a result of this

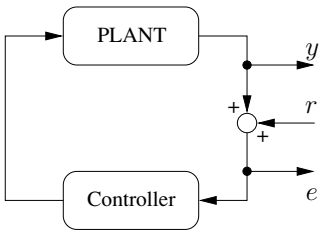

Figure 10. Setup used to measure the closed-loop step response. In this block diagram, r represents the step disturbance signal which is introduced into the control system and the resulting step response of the system is the measured signal y.

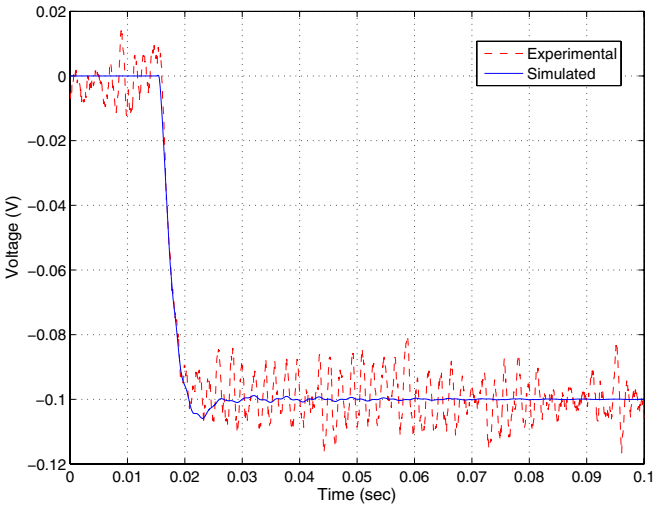

Figure 11. Step response of the closed-loop system to a step input disturbance of magnitude 0.1 V. This step disturbance is applied to the control system as shown in figure 10. In this diagram, the measured step response is compared with the simulated step response obtained using the identified plant model.

disturbance, as well as to show that the experimental system behaves as predicted by the theory.

The experimentally measured step response is shown in figure 11 and is compared with the corresponding simulated step response obtained by using the identified plant model and the designed controller.

Having demonstrated that the LQG design methodology can yield a working cavity-locking system with performance consistent with its theoretical description, what remains is a discussion of the relative merits of the traditional and LQG controller design methodologies. The fundamental limits to the performance of the closed-loop system still apply, irrespective of the controller design methodology. That is because the basic physical principles that set those fundamental limits are unchanged by the methodology used to design the controller. So the power of the LQG design methodology lies in the way in which the performance of the closed-loop system is engineered given a set of practical limitations and constraints.

To be more specific, the ultimate limits to metrics such as the linewidth, Allan variance on long and short timescales, pointing stability or intensity noise of the closed-loop system are still set by the same physical limits of cavity locking. Such performance metrics depend on things such as the power of the laser, the noise-floor of the laser and the linewidth of the frequency discriminator. But those ultimate limits assume that there is no limitation to the energy that can be supplied by the controller and they are premised on the assumption that a stable controller can be designed for that particular plant. Because of those assumptions, calculations that lead to predictions of the ultimate limits of cavity-locking systems provide no guidance as to how to go about designing a controller that might achieve those limits while still being stable and robust.

By contrast, the practical limits to the performance of the closed-loop system, as measured by metrics such as the unity-gain bandwidth, gain margin and phase margin, depend intimately on the controller design methodology. Cavity-locking controller design is traditionally done by hand, making use of Bode plots, root-locus methods and Nyquist diagrams [19]. As a general rule, controller designs start off as some combination of the standard set of proportional, integral and differential transfer functions. A critical point here is that the final controller design depends on a number of engineering trade-offs and the quality of the final product depends on the imagination and experience of the individual designer. On the other hand, systematic approaches to controller design, of which LQG is just one, codify the engineering trade-offs in the state-space model of the plant as well as in the cost functional. In our case, the engineering trade-offs were codified in the choice of design parameters listed in table 1 and in the choice of an integral-LQG cost functional. An LQG controller often can have better performance than a traditionally designed one, simply by virtue of not being confined to a modified proportional-integral-differential architecture. Finally, systematic controller design methodologies guarantee the optimality of the solution for a given set of engineering trade-offs.

7. Conclusion and future work

In this paper, we have shown that a systematic modern control technique such as the LQG integral control can be applied to a problem in experimental quantum optics which has previously been addressed using traditional approaches to controller design. From frequency response data gathered, we have successfully modelled the optical cavity system and used an extended version of the LQG cost functional to formulate the specific requirements of the control problem. A controller was obtained and implemented which locks the resonant frequency of the cavity to that of the laser frequency.

The ultimate performance of a cavity-locking system is still limited by the underlying physics of the system. But a variety of metrics such as the unity-gain bandwidth, gain and phase margins, are dominated by more pragmatic considerations. Cavity-locking controllers are traditionally designed by hand and their performance relies on the imagination and skill of the individual designer. By contrast, the LQG cavity-locking controller design methodology codifies those pragmatic considerations, returns a controller design and guarantees that the resulting design is optimal within the imposed constraints.

Another important advantage of the LQG technique is that it can be extended in a straightforward way to multivariable control systems with multiple sensors and actuators. Moreover, the subspace approach to identification used here is particularly suited to multivariable systems. It is our intention to further the current work by controlling the laser pump power using a similar scheme as that used in this paper. This work is expected to pave the way for extremely stable lasers with fluctuations approaching the quantum noise limit and which could be potentially used in a wide range of applications in high precision metrology, see [37].

Acknowledgment

This work was supported financially by the Australian Research Council.

References

[1] Ahn C, Doherty A C and Landahl A J 2002 *Phys. Rev.* A **65** 042301
[2] Yanagisawa M and James M R 2008 *Proc. 17th IFAC World Congress (Seoul, Korea)* pp 8996–9001
[3] Hopkins A, Jacobs K, Habib S and Schwab K 2003 *Phys. Rev.* B **68** 235328
[4] Yamamoto Y, Imoto N and Machida S 1986 *Phys. Rev.* A **33** 3243–61
[5] Drever R W P, Hall J L, Kowalski F, Hough J, Ford G M, Munley A J and Ward H 1983 *Appl. Phys.* B **31** 97
[6] Hänsch T W and Couillaud B 1980 *Opt. Commun.* **3** 441
[7] Doherty A C and Jacobs K 1999 *Phys. Rev.* A **60** 2700
[8] Edwards S C and Belavkin V P 2005 arXiv:quant-ph/0506018
[9] James M R, Nurdin H I and Petersen I R 2008 *IEEE Trans. Autom. Control* **53** 1787
[10] Mabuchi H 2008 arXiv:0803.2007v1 [quant-ph]
[11] Shir O M, Beltrani V, Bäck Th, Rabitz H and Vrakking M J J 2008 *J. Phys. B: At. Mol. Opt. Phys.* **41** 074021
[12] Grimble M J 1979 *Proc. IEE* D **126** 841
[13] Kwakernaak H and Sivan R 1972 *Linear Optimal Control Systems* (New York: Wiley)
[14] McKelvey T, Akçay H and Ljung L 1996 *IEEE Trans. Autom. Control* **41** 960
[15] Bachor H and Ralph T 2004 *A Guide to Experiments in Quantum Optics* 2nd edn (Weinheim: Wiley)
[16] Gardiner C and Zoller P 2000 *Quantum Noise* (Berlin: Springer)
[17] Kogelnik H and Li T 1966 *Appl. Opt.* **5** 1550
[18] Siegman A E 1986 *Lasers* (Mill Valley, CA: University Science)
[19] Dorf R C and Bishop R H 1995 *Modern Control Systems* 7th edn (Reading, MA: Addison-Wesley)
[20] van Overschee P and De Moor B 1996 *Subspace Identification for Linear Systems* (Dordrecht: Kluwer)
[21] Ho B and Kalman R 1966 *Regelungstechnik* **14** 545
[22] Kung S 1978 in *Proc. 12th Asilomar Conf. on Circuits, Systems and Computers (Pacific Grove, CA)* pp 705–14
[23] Gopinath B 1969 *Bell Syst. Tech. J.* **48** 1101
[24] Moor B D, Vandewalle J, Vandenberghe L and Mieghem P V 1988 *Proc. IFAC Symp. on System Identification (Beijing)* pp 700–4
[25] Lin K, Jacques R N and Miller D W 1994 *Proc. American Control Conf.* vol 1 (Baltimore, MD) pp 107–11
[26] McKelvey T 1994 *Proc. American Control Conference* (Boston, MA) pp 673–8
[27] Burden R L and Faires J D 1989 *Numerical Analysis* 4th edn (Boston, MA: PWS-KENT Publishing Company)
[28] Astrom K J and Wittenmark B 1997 *Computer Controlled Systems* 3rd edn (Upper Saddle River, NJ: Prentice-Hall)
[29] Kalman R E 1960 *Bol. Soc. Mat. Mex.* **5** 102
[30] Kalman R E 1960 *Trans. ASME* D **82** 35
[31] Kalman R E and Bucy R S 1961 *Trans. ASME* D **83** 95
[32] Astrom K J 1970 *Introduction to Stochastic Control Theory* (New York: Academic)
[33] Anderson B D O and Moore J B 1990 *Optimal Control: Linear Quadratic Methods* (Englewood Cliffs, NJ: Prentice-Hall)
[34] Cheng Y-J, Mussche P L and Siegman A E 1994 *IEEE J. Quantum Electron.* **30** 1498
[35] Zhou K, Doyle J and Glover K 1996 *Robust and Optimal Control* (Upper Saddle River, NJ: Prentice-Hall)
[36] Sayed Hassen S Z, Huntington E, James M R and Petersen I R 2008 *Proc. 17th IFAC World Congress (Seoul, South Korea)* pp 1821–6
[37] Huntington E H, Harb C C, Heurs M and Ralph T C 2007 *Phys. Rev.* A **75** 013802